Numerical and Experimental Investigation of Helicopter Fuselage Aerodynamics

Rhys Lehmann, Rami Reddy and Steve Armfield[†]

Air Operations Division
Defence Science and Technology Organisation
506 Lorimer St, Fishermans Bend, Victoria, Australia

[†]School of Aerospace, Mechanical and Mechatronic Engineering
The University of Sydney, New South Wales, Australia

Abstract

The aerodynamic characteristics of an isolated MRH 90 helicopter fuselage have been investigated using Computational Fluid Dynamics (CFD). Simulations utilised an unstructured tetrahedral grid and both the k-ε and k-ω SST turbulence models were investigated. Standard 'law of the wall' wall functions were incorporated, along with a segregated finite volume solver. A wind tunnel testing program was also undertaken to provide a benchmark for comparison. Reasonable levels of agreement were obtained between numerical and experimental results, with the majority of cases falling within ten percent. Prediction of drag values was found to be the most difficult, which is likely to be a function of the inability to fully resolve the boundary layer. It was proposed that errors in lift and side forces at extreme orientations could result partially from wind tunnel support interference effects.

Introduction

Flight dynamic models enable research in support of Australian Defence Force (ADF) aircraft operations. These models are used to fulfil a wide range of roles, from operational analysis and training to Human Machine Interface research and accident investigation. Construction of high fidelity flight dynamic models is only possible if detailed knowledge of aircraft aerodynamic and dynamic characteristics of the various elements is available. One such component for a rotary wing aircraft is the fuselage.

Helicopter fuselage aerodynamics have a significant effect on performance and flight characteristics, particularly in forward flight. While comprehensive knowledge of this data is often gained throughout the development and testing phases, manufacturers can be reluctant to release such information as it represents a significant investment of time and money. In these cases this data needs to be obtained using alternate means.

Numerical and experimental aerodynamic techniques both present themselves as possible solution methods for the generation of the required data. This study involves the analysis of the aerodynamic characteristics of an isolated MRH 90 fuselage using Computational Fluid Dynamic (CFD) techniques. The MRH 90 is a medium lift utility helicopter developed by NH Industries, currently being acquired by the ADF as part of the AIR 9000 project.

Numerical simulations were performed over a range of low angle of attack and sideslip combinations at a single fixed airspeed. A wind tunnel testing program was also undertaken on a 1/30th scale model in an equivalent configuration in order to establish the degree of accuracy of the numerical simulations. Comparison of resulting forces and flow structures between the two techniques was performed.

Simulation Setup

The commercial solver ANSYS FLUENT was utilised, with the primary focus being on the k-ω Shear-Stress Transport (SST) and k-ε turbulence models. A 'cleaned up' CAD model of the MRH 90 Fuselage was analysed, with the rotor hub, tail and boom, undercarriage and external accessories removed.

The mesh was generated using the commercial meshing tool GAMBIT. An unstructured tetrahedral grid was utilised, with an average surface y+ of 50, which is used to define a non-dimensional distance from the wall. Standard logarithmic 'law of the wall' functions were used on the model surface. Due to the limited amount of available computer hardware, the mesh was split into sections to improve efficiency. The model and immediate surroundings were placed within a small box, which contained the smallest cells with a low expansion ratio. The outer regions were split into two sections, both having much higher growth rates. This effectively limited the number of cells and resulting memory requirements for each individual meshing operation, allowing a larger mesh to be generated. Significant refinement was performed behind the model in order to capture the behaviour of the wake. The mesh close to the model is shown in Figure 1.

The final simulation runs were performed using the k-ω turbulence model, using the SST correction by Menter. This model uses a blending function to transition into the k-ε model in k-ω form in the free shear layer, which reduces the sensitivity to free stream values of ω [1]. The outer domain dimensions were set to match those of the wind tunnel used in experiments, and the flow was consistently aligned within the domain. Flow angles were generated by rotating the model about its pitch and roll axes in a similar fashion to the experimental set up. This allowed the domain size and refined wake regions to remain the same for all orientation angles, but did require that the meshing process was repeated for each case.
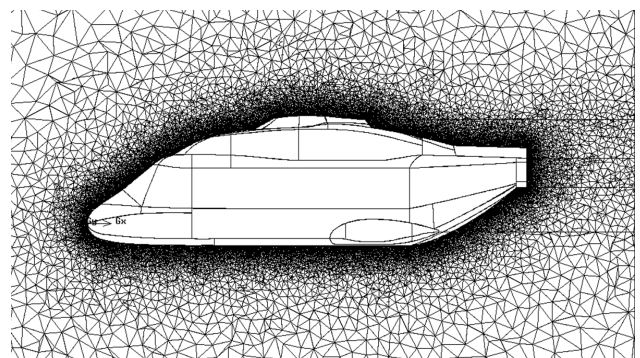

Figure 1: Mesh close to model surface

The inlet boundary condition specified similar turbulence intensity conditions to measured values in the wind tunnel, and the length scale was based upon the domain size. Outlet conditions were constrained using a Fluent outflow.

Simulations were performed using Fluent's segregated finite volume solver, using a SIMPLE pressure correction method. This uses a pressure correction factor and iterates to obtain a conservative solution [2]. First order upwind advection schemes were required for a fully convergent solution to be obtained. It is likely that further mesh refinement would be required for higher order schemes to be used successfully.

While grid independence was not able to be obtained within the available hardware constraints, mesh dependency studies showed that for a 15% increase in the number of cells around the surface the variations in forces were less than two percent. As was mentioned earlier, the dimensions of the outer domain matched those of the wind tunnel, and studies showed that the inlet and outlet were sufficiently far away from the model to have minimal effects on the final solution. Overall variations in drag results between the k-ε and k-ω SST turbulence models were found to be in the order of 15%, with the k-ε model consistently over predicting pressure drag and slightly under predicting viscous drag when compared to the k-ω SST model. This also meant that variations of up to five percent were present in the lift and side forces between the two models. The drag results for the two turbulence models are presented in Figure 2. The wind tunnel results are included for comparison.

Experimental Setup

Wind tunnel testing was performed in the 7' x 9' DSTO Low Speed Wind Tunnel (LSWT). The model was constructed of polycarbonate, using an identical geometry to the one used in the numerical simulations, which was approximately 1/30th scale. A detachable tail was incorporated in the model, allowing testing to be run both with and without the tail. The six component force and moment balance was located within the model, which was mounted from behind using a sting column. Aerodynamic angles were achieved using various combinations of pitch and roll about the sting column axes, and the test matrix covered a range of approximately ±30° angle of attack and sideslip. The tunnel was run at 70m/s and transition strips were used around the nose in an attempt to ensure a fully turbulent solution. Smoke visualisation was used at the end of the testing program to observe the location of dominant vortices and other major flow characteristics.
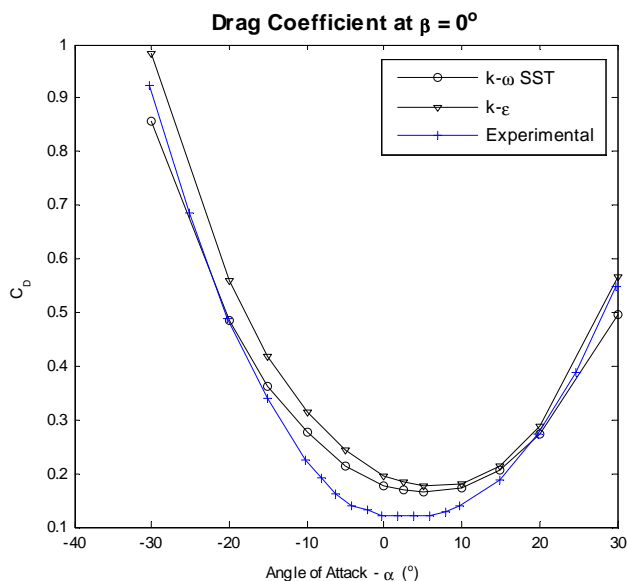
Results

The results for drag, lift and side force coefficients are shown in Figures 3 to 7 for various angles of attack and sideslip. Simulated results were generated using the k-ω SST model. Drag and lift are presented as a function of angle of attack (α), while side force is shown as a function of sideslip angle (β).

At low angles of sideslip, simulated and experimental drag results show some discrepancies, particularly between -15° and 10° angle of attack. This can be seen in the 0° sideslip case in Figure 3. The highest variations are present at approximately -5° angle of attack. The wind tunnel results appear to have a flat section between 0° and 5°, moving the point of lowest drag closer to 0°. This does not appear to be replicated in the numerical results, with the lowest drag occurring at around 5° angle of attack.

As the magnitude of angle of attack increases, the error between the two sets of results decreases significantly, reaching zero at ±20°. At ±30° angle of attack some errors reappear, however these remain within 10% as the overall magnitude of the drag coefficient has increased. It appears that for low angles of sideslip the predicted drag curve has a lower slope than experimental results. This suggests that at more extreme angles of attack the errors are likely to continue increasing.

At 20° of sideslip the simulated drag at zero angle of attack matches the numerical results quite closely, as is shown in Figure 3. Lowest drag occurs for both at around 5°, and a flat portion is no longer observed in the low angle of attack region of the experimental results. As the angle of attack moves above 10° or below 0°, discrepancies between the measured and predicted results emerge, increasing proportionally with the magnitude of the angle. The calculated results appear to consistently under-predict drag at high angles of sideslip. This once again points to the simulated results under predicting the drag slope.

Comparison of the lift coefficient at low angle of sideslip was found to show high levels of agreement for all angles of attack, as can be seen in Figure 4. Even at the most extreme angles, differences were less than 10%. Lift results were composed of two key sections, high and low angle of attack. For small magnitudes of angle of attack, the lift curve slope was at its lowest, while the highest slopes were found at extreme angles of attack. Both regions were essentially linear, and a smooth change in slope was present between the two regions.
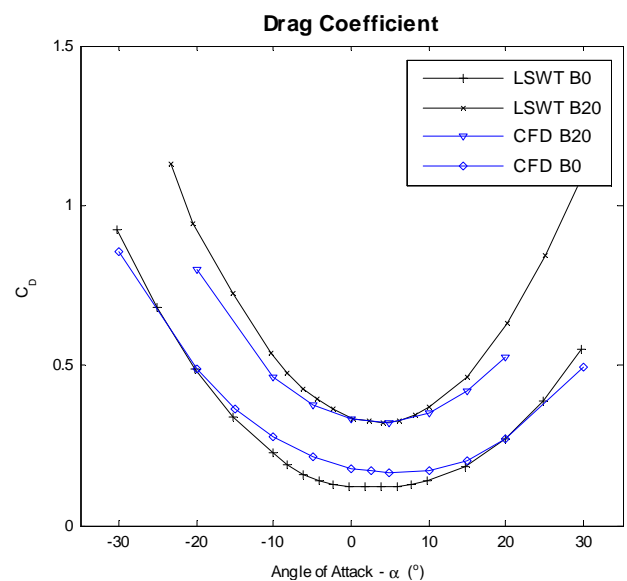

Figure 2: Drag Coefficient results for k-ω SST and k-ε turbulence models at zero degrees sideslip.

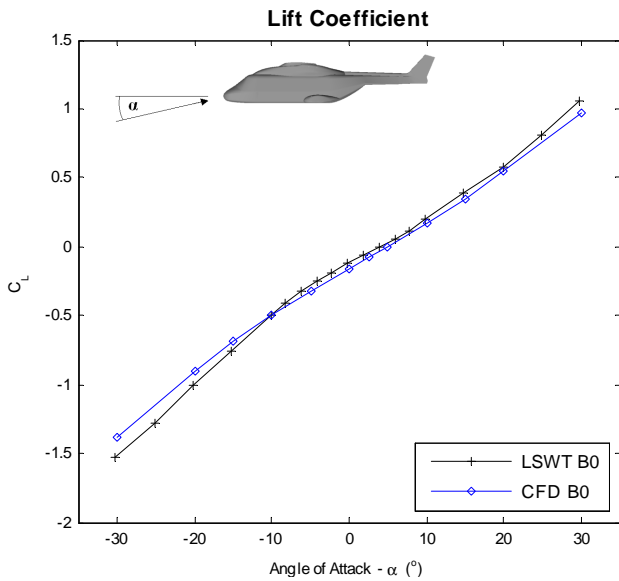

Figure 3: Drag Coefficient at high (β=20°) and low (β=0°) angles of sideslip

Figure 4: Lift Coefficient at low sideslip angle (β=0°)
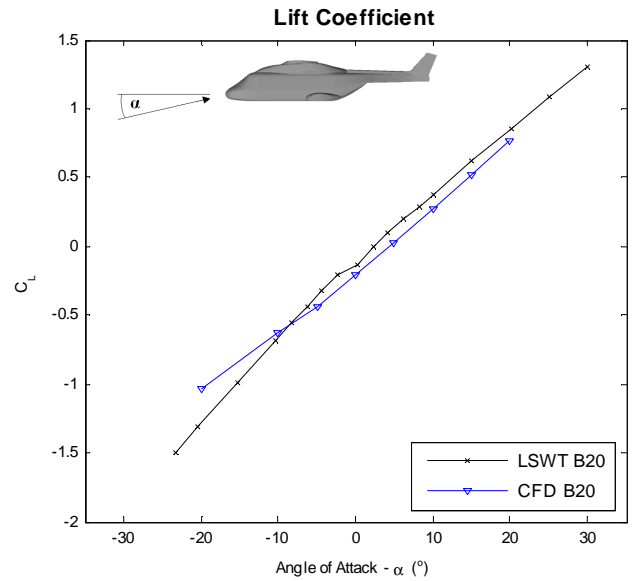

Figure 6: Lift Coefficient at high sideslip angle (β=20°)
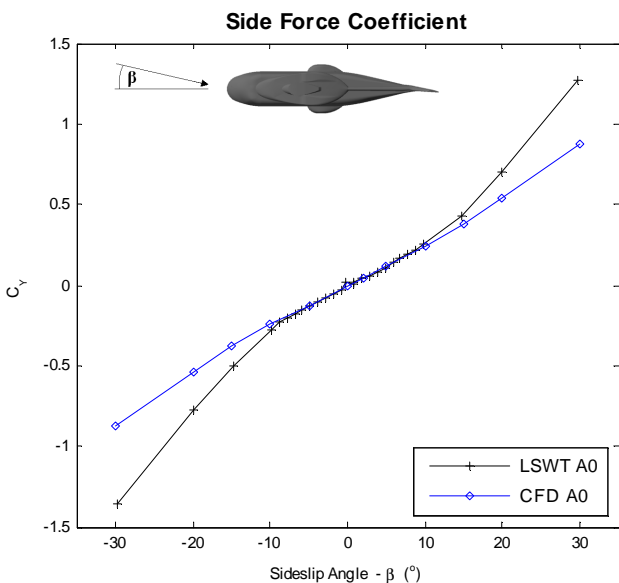

Figure 5: Side Force Coefficient at low angle of attack (α=0°)

Figure 7: Side Force Coefficient at high angle of attack (α=20°)

At high angles of sideslip, an almost constant difference is apparent between the simulated and experimental results for angles of attack larger than 10°, as can be seen in Figure 6. This corresponds to a shift to the right of the zero lift angle of attack from approximately 3° to 5°. At lower angles of attack the experimental results show a consistently lower lift curve slope than the numerical results. The lift curve slope of the simulated results appears to decrease slightly at below -5° angle of attack, while the experimental results show a distinct increase.

Numerical and experimental side force results showed excellent agreement at low angle of attack between ±10° sideslip, as can be seen in Figure 5. Side forces were symmetrical about the sideslip axis for both cases. In a similar fashion to the lift results, two key sections were evident in the side forces depending on the sideslip angle. Moderate angles had the lowest slope while the more extreme angles showed the highest gradients. At high angles of sideslip the agreement between the simulated and experimental results was poor, as the two had quite different gradients. This change in slope was considerably more noticeable than in the lift results, while the variations between the two methods at moderate sideslip angle were lower than in the lift.
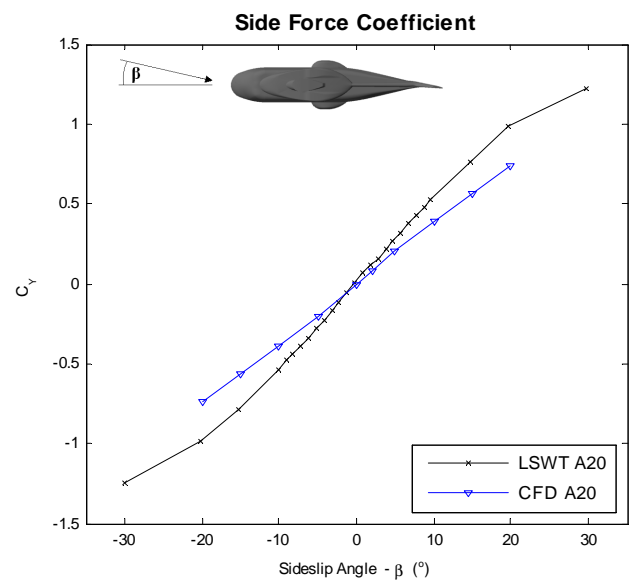
At high angle of attack the side force trends were reversed, with the highest gradients experienced at low magnitudes of sideslip angle. In these cases, the numerical results showed consistent under-prediction with respect to experimental results for all sideslip angles, as can be seen in Figure 7.

The variations between experimental and simulated moment results followed similar trends to those exhibited in lift and side forces, and due to space limitations have not been presented here. In general, pitching moments showed reasonable agreement at low angles of attack, but did not agree well at high angles. Similarly, yawing moments matched almost exactly at low angles, but the same divergence characteristics appeared as in the side forces. Rolling moments were deemed to not have physical significance and as such were not considered in detail.

Discussion

It was found that the flow structures could be separated into two distinct cases. The first was at low magnitudes of angle of attack and sideslip, where the generated lift and side forces were of a relatively low magnitude, and the second was at more extreme angles (beyond ±15°). At extreme angles, strong vortices were released from the wheel fairings and the rear of the rotor hub.

These can be seen in Figure 8, showing a vector plane of flow velocity perpendicular to the flow at the rear of the model. The model was at a negative angle of attack. As can be seen, in this case two sets of vortices are produced. The inner pair result from the flow travelling from the lower portion of the tail into the wake directly behind the model. The outer pair result from the flow travelling around the wheel fairings further forward on the model. As can be seen, these have a much greater effect on the overall flow field. The flow was found to reverse direction as it passed around the rotor fairing at the top of the model, which combined with the vortices generated from the wheel fairings.
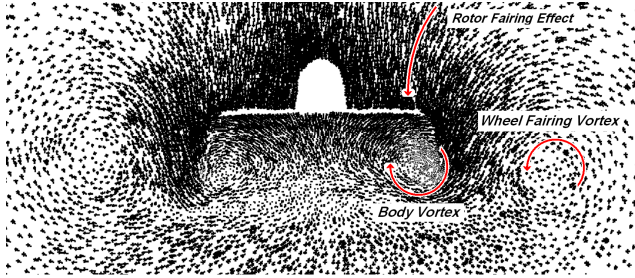

Figure 8: Flow Structures in Vertical Plane at Rear of Model (α = -15°)

It was found that these vortices allowed the flow to remain attached on the rear surfaces even at very high angles of attack. It is probable that this behaviour explains the apparent transition in lift curve slope witnessed in both the lift and side forces at around ±10°. As the angle of attack increases beyond this value, two things occur. Firstly, the amount of generated lift becomes sufficient to create enough of a pressure differential between the upper and lower surface to produce a pair of strong vortices, originating from the lower surface. Secondly, the model orientation is such that these vortices pass directly over the rear of the upper surface of the model, which appears to prevent flow separation. The same processes occur at negative angles of attack, however in this case two sets of vortices are generated as the flow travels around the rotor hub and the wheel fairings. This allows the transition from the first case to the second to occur at a lower magnitude of angle of attack. Similar processes also occur as the sideslip angle increases.

The most significant variations in drag results between the wind tunnel and simulations were experienced at low angle of attack and sideslip. In this region, the pressure component of drag is of a similar magnitude to the viscous drag. It is likely that the use of wall functions lead to increased levels of diffusivity in the boundary layer, increasing the component of viscous drag. As the angle of attack and sideslip increases, the pressure component becomes much more dominant, leading to more accurate drag predictions. It appears that at high angles of attack and sideslip the simulations are tending to under predict drag. This is most likely predominately due to the variations in lift and side forces, as is discussed in the following section. The lower forces predicted by the simulations produce smaller vortices, hence reducing the amount of pressure driven induced drag. These two effects appear to cancel each other out in the case of high sideslip and low angle of attack, as can be seen in the 20° sideslip curve in Figure 3.

The k-ε turbulence model was found to consistently over-predict drag when compared to the k-ω SST model. It is likely that this occurred as a result of the tendency of k-ε model to over predict the turbulence length scale in the near wall regions [3].

In contrast to drag results, lift and side force results agree best at low angles of attack and side slip. In this case, the contributions of viscous forces to lift and drag are minimal. At extreme angles of attack and sideslip, the predictions were found not to be very accurate. While it has not been possible to prove this, it has been proposed that the interference effects of the sting column in the wind tunnel could have significantly disrupted the flow in the wake of the model. The sting would have been most exposed at extreme angles, and is likely to have had two effects. The first would be a modification of the pressure field in the wake, potentially leading to differing amounts of lift and side forces being produced. The second effect would have been a blockage effect, with the sting possibly preventing the flow from passing across the rear of the model. In the case of extreme angles of attack and moderate sideslip, this would have prevented the flow from passing from the lower surface to the upper, or vice versa. As can be seen from Figure 8, a significant vertical component of flow is present across the lower back end of the model, largely as a result of the combination of vortices. This would have been significantly reduced with the addition of the sting column, leading to an increase in the magnitude of the overall lift as the supports became more exposed. This effect is likely to have been even more pronounced in the side forces, as the lower rear portion of the model, which in the experiments housed the sting, was flat. This appears to be supported by the observed results. Experimental values of lift and side force were of a significantly higher magnitude in the extreme angles, where the exposure of the sting column and vortex activity were greatest. Further clarification of these effects could be obtained by either performing further wind tunnel analysis to investigate support interference effects, or modifying the CFD model to more closely model the experimental configuration.

Concluding Remarks

A combined experimental and numerical study was performed on the aerodynamic characteristics of the isolated fuselage of the MRH 90 helicopter. Results of this study are to be utilised to improve the fidelity of future flight dynamic models for the aircraft. Numerical simulations were performed using a commercial CFD package with an unstructured mesh, and experimental testing was done using a low speed wind tunnel. While memory constraints dictated the degree of mesh resolution and resulting degree of accuracy that could be obtained in the numerical solution, reasonable levels of agreement were achieved over the majority of the angle of attack and sideslip range.

Drag predictions were best in the moderate to high angle combinations, and it was concluded that the primary limitation was the inability to properly model the viscous forces using wall functions. Lift and side forces were found to show highest agreement at low angles, with significant increases in levels of error at extreme angles. It was proposed that wind tunnel support effects may have played a major role in this.

It was found that vortex activity became the dominant flow characteristic above angles of attack and sideslip of around ±15°. This was demonstrated in the wind tunnel experiments, and predicted in a similar fashion using CFD.

Future work would include improving the numerical model to more closely represent the experimental configuration, with possible scope for further experimental runs to investigate the support interference effects. It could also include development of the numerical configuration in order to better match the full scale characteristics of the aircraft.

References

[1] Menter, F. R. *Zonal Two Equation k-ω Turbulence Models for Aerodynamic Flows*, AIAA Paper 93-2906, 1993

[2] FLUENT Inc: *Fluent 6.2 Documentation*, 2005

[3] Wilcox, D. C. *Turbulence Modelling for CFD*, DCW Industries, Inc. 1994